Aeroacoustic sources of motorcycle helmet noise

J. Kennedy,[a] O. Adetifa, and M. Carley
Department of Mechanical Engineering, University of Bath, Bath, BA2 7AY, United Kingdom

N. Holt
School of Science, Society and Management, Bath Spa University, Newton Park, Newton Street Loe, Bath, BA2 9BN, United Kingdom

I. Walker
Department of Psychology, University of Bath, Bath, BA2 7AY, United Kingdom

(Received 8 February 2011; revised 27 June 2011; accepted 5 July 2011)

The prevalence of noise in the riding of motorcycles has been a source of concern to both riders and researchers in recent times. Detailed flow field information will allow insight into the flow mechanisms responsible for the production of sound within motorcycle helmets. Flow field surveys of this nature are not found in the available literature which has tended to focus on sound pressure levels at ear as these are of interest for noise exposure legislation. A detailed flow survey of a commercial motorcycle helmet has been carried out in combination with surface pressure measurements and at ear acoustics. Three potential noise source regions are investigated, namely, the helmet wake, the surface boundary layer and the cavity under the helmet at the chin bar. Extensive information is provided on the structure of the helmet wake including its frequency content. While the wake and boundary layer flows showed negligible contributions to at-ear sound the cavity region around the chin bar was identified as a key noise source. The contribution of the cavity region was investigated as a function of flow speed and helmet angle both of which are shown to be key factors governing the sound produced by this region. © *2011 Acoustical Society of America*.
[DOI: 10.1121/1.3621097]

PACS number(s): 43.28.Ra, 43.50.Nm, 43.50.Lj [AH] Pages: 1164–1172

I. INTRODUCTION

Noise inside motorcycle helmets has been recognized as a hearing hazard for just over 20 years, since the first extensive studies were conducted by police forces in the Netherlands[1–4] and the United Kingdom.[5,6] Since then it has been understood that noise in helmets is dominated by the aerodynamic sources caused by flow over the helmet, and there have been a number of published measurements of noise levels inside helmets[7] (for example), reflecting the desire to educate motorcyclists in the need to protect their hearing.[8]

Despite the work which has been done on measuring noise inside helmets, there are relatively few data in the open literature on the mechanisms of noise generation or on the nature of the noise. The flow on, and around, the helmet is the noise source responsible for hearing damage. As part of a study on noise inside helmets a flow survey of a commercial motorcycle helmet has recently been conducted. This survey had the aim of establishing the main features of the flow which are, or might be, responsible for noise generation. Other factors which must be considered are propagation of noise from the source through the helmet and head of the rider, but without a knowledge of the source, little can be done to control the noise.

To gain some insight into the features which might be expected in a flow survey of a motorcycle helmet we consider flow around spherical bodies. Data for flow around a sphere at Reynolds numbers similar to those in our tests have been published by Taneda[9] and by Achenbach.[10,11] These are useful in establishing broad parameters for the flow over isolated helmets, although it may be that a better approximation for the geometry of a rider is a form such as an ellipsoid, but there are few data on the aerodynamic processes which give rise to noise in and around the surface of bodies comparable to helmets.

An issue which is not considered in this paper is the effect of the rider's body and of the motorcycle structure, in particular the fairing or windscreen. We have studied these effects elsewhere, however, and have found that while the windscreen does have an effect on noise in the helmet, depending on head position,[12] wind-tunnel measurements on an isolated head model do accurately reproduce the noise measured on a real rider on the road.[13] In this other work, studies were conducted on two different helmets, including that used in an earlier on-road study,[14] and it was found that the noise measured in both cases was very similar, even though the helmets were quite different in their external features. We conclude that the details of the helmet make little difference to the noise and assume that our results are general.

From published data, however, some general conclusions can be drawn. The Reynolds number for a sphere of diameter $D = 300\,\text{mm}$ at free stream velocity of 80 km/h ($U_m = 22\,\text{m/s}$) is $\text{Re} = U_m D/\nu \approx 4.5 \times 10^5$. Boundary layer separation on a smooth sphere at this Reynolds number occurs at $\phi \approx 120°$ from the inflow axis while the transition to turbulent flow has been shown[10] to occur at $\phi \approx 95°$. The same

[a]Author to whom correspondence should be addressed. Electronic mail: kennedj@tcd.ie.

work also reports a characteristic Strouhal number $St = fD/U_m = 0.18$ at this Reynolds number. Given that a motorcycle helmet is not a smooth sphere in a uniform flow, we would expect both separation and transition to occur earlier but these figures are useful indications of what to expect. On the downstream side of a sphere, flow visualization studies at the relevant Reynolds numbers[9] show evidence of a vortex sheet shed from the back of the sphere to generate a vortex pair. For $Re > 5 \times 10^5$, this feature oscillates randomly through less than 180°. We might expect to see such a feature in these tests, though probably at lower Reynolds number.

II. EXPERIMENTAL FACILITIES AND INSTRUMENTATION

The large wind tunnel facility at the University of Bath was used for all tests. This closed loop facility has a 2 m × 1.5 m × 3 m test section and can provide flow velocities up to 25 m/s with a freestream turbulence intensity of 0.1%. In order to compare the results of wind tunnel tests with future on-road data three flow speeds were chosen which are representative of driving conditions, namely, 11, 16.5, and 22 m/s equivalent to road speeds of 40, 60, and 80 km/h. The motorcycle helmet was mounted on the structurally isolated α rig, a system which varies the incidence angle of the helmet relative to the free stream. This provides dynamic control of helmet position while isolating the helmet from any wind tunnel vibrations. The blockage ratio caused by the helmet and α rig was 16%. Figure 1 shows the setup within the wind tunnel.

The helmet used in this investigation is one of a number of helmets provided by manufacturers for noise investigations. As such, the make and model are covered by a confidentiality agreement. It is a commercially available extra large (XL) motorcycle helmet and was mounted using an expanded polystyrene mannequin head the dimensions of which are given in Table I. The majority of the mannequin head measurements correspond to the 50th percentile for adult males according to the NASA Man-Systems Integration Standards.[15] The helmet dimensions were 26 cm × 25 cm × 36 cm. The helmet featured numerous air vents and an aerodynamic wing on the back surface commonly found on many high end motorcycle helmets. This paper investigates the importance of three

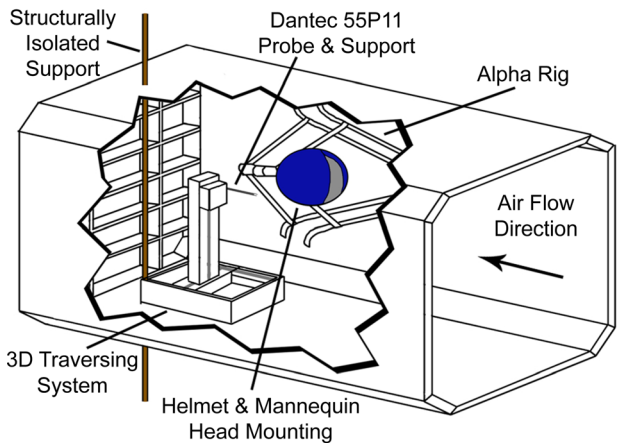

FIG. 1. (Color online) Wind tunnel facility.

TABLE I. Mannequin head dimensions.

Dimension	
Face breadth	14.0 cm
Head length	19.5 cm
Face length	11.5 cm
Head breadth	16.5 cm
Head circumference	29.0 cm

potential sound producing regions of the flow, namely, the helmet wake, the surface boundary layer and the cavity region beneath the helmet rim.

The flow measurements were acquired using a calibrated Dantec 55P11 hot wire probe and a DISA type 56C01 CTA unit with a DISA type 56C16 CTA bridge. The probe was mounted in a three axis traverse system controlled by dedicated Labview software. The wake flow was investigated using two separate test grids. The first grid assessed flow symmetry and consisted of 5 horizontal traverses of the hot wire as shown in Fig. 2. Due to the complexity of the flow region to be measured and the symmetric shape of the helmet a second detailed grid extending from the free stream to 1 cm past the midpoint of the helmet was also used. The second grid consisted of 451 points and was designed with varying spatial resolution for a smooth transition from the free stream to the turbulent wake of the helmet. Measurements were acquired using this grid at four locations of increasing distance from the back surface of the helmet. These locations were chosen based on the helmet length as $Z/L = 0, 0.25, 0.5,$ and 1.0. Figure 3 shows the grid point locations relative to the helmet. Boundary layer measurements were made at the helmet surface adjacent to the right ear and at a position at the top of the helmet.

Further measurements were acquired using 1/4 inch 130D20 PCB Piezotronics microphones connected to a PCB 442B117 signal conditioner. These were calibrated using a Larson Davis CAL200 microphone calibration unit. Surface pressure fluctuations were acquired using two flush mounted

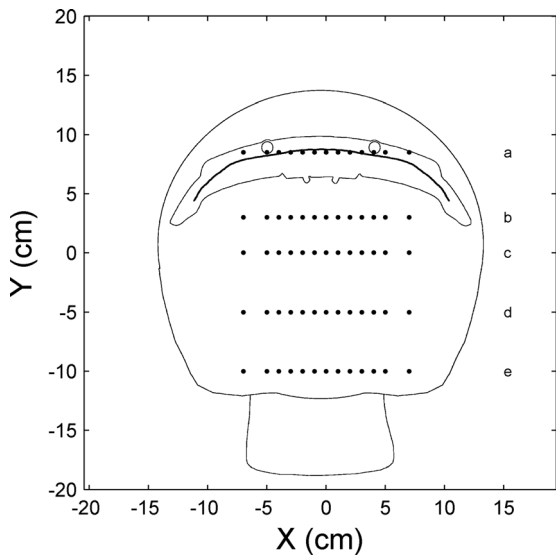

FIG. 2. Grid 1 hot wire measurement locations.

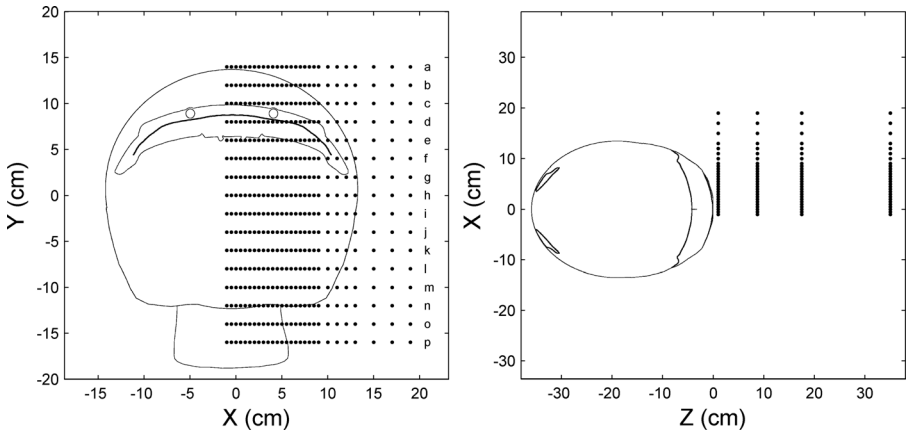

FIG. 3. Grid 2 hot wire measurement locations.

microphones in the helmet visor. The microphones used were located 12 cm from the visor center at eye level. The sound produced by the cavity under the helmet rim was investigated using a microphone located at the helmet chin bar. Sound pressure levels and spectra at ear were acquired using two microphones mounted within the mannequin head.

In order to quantify and remove the effects of tunnel noise a sixth $1/4$ inch PCB microphone was mounted upstream of the α rig within the wind tunnel. The hot wire and PCB microphone data were acquired using a 16 channel NI DAQ system. This system comprised a PC with a NI-PCI-MIO-16E-1 acquisition card and BNC-2090 connector box.

III. SIGNAL CONDITIONING

The wind tunnel used has no acoustic treatment meaning that there is a risk of signal contamination by spurious background noise. Also, we wish to compare wind tunnel measurements to data taken on a motorcycle where there is a contribution to the in-helmet noise from the motorcycle engine and from environmental sources. In order to extract a "helmet-only" spectrum, one which contains only the noise due to flow over the helmet, we apply a signal conditioning procedure which has been used in a number of applications[16,17] to conditionally remove unwanted contributions to the output signal.

A model for the system is shown in Fig. 4. The output signal $p(t)$ is composed of a sum of inputs $g_i(t)$, $i = 1, 2, \ldots$. If we consider a two input problem, where $g_1(t)$ is a background noise contribution to $p(t)$ and $g_2(t)$ is the "real" aerodynamically generated noise in the helmet, we wish to remove from $p(t)$ the part of the signal which is correlated with $g_1(t)$. This is readily done using standard signal processing methods. If we wish to remove the effects of multiple signals, however, we must take account of possible correlations between them. In this case, if we wish to remove the contributions of $g_i(t)$, $i = 1, 2$, leaving the "true" signal due to $g_3(t)$, we cannot simply remove from $p(t)$ the part which is correlated with $g_1(t)$ and/or $g_2(t)$. Instead, we must decorrelate the input signals before proceeding.

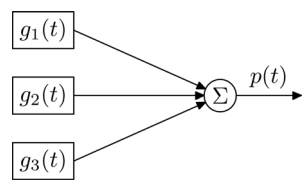

FIG. 4. System model for partial coherence processing.

The method of partial coherence is a systematic technique for performing this decorrelation in order to rigorously assess the contribution of different sources. If the inputs are uncorrelated, the coherence function of each with the output signal is

$$\gamma_{ip}^2(f) = \frac{|G_{ip}(f)|^2}{G_{ii}(f)G_{pp}(f)},$$

where $G_{pp}(f)$ is the autospectrum of $p(t)$, $G_{ii}(f)$ is the autospectrum of $g_i(t)$ and G_{ip} is the corresponding cross-spectrum. The contribution of the ith source to the output can then be removed by subtracting the correlated part:

$$G_{pp.i} = (1 - \gamma_{ip}^2)G_{pp}. \tag{1}$$

The notation $G_{pp.i}$ denotes the spectrum of the signal $p(t)$ with the contribution of the ith input removed.

If the input signals are correlated, however, this procedure is not valid, as it will lead to a correlated part being subtracted more than once. In this case, the input signals must be processed to make them mutually uncorrelated. This is done by using a recursive conditioning procedure, treating each signal in turn:

$$G_{pp.i} = \left[1 - \gamma_{ip.(i-1)!}^2\right] G_{pp.(i-1)!}. \tag{2}$$

Here, $G_{pp.(i-1)!}$ is the power spectrum of $p(t)$ with the correlated part of all inputs up to $i-1$ removed and the partial coherence $\gamma_{ip.(i-1)!}^2$ given by

$$\gamma_{ip.(i-1)!}^2 = \frac{|G_{ip.(i-1)!}|}{G_{ii.(i-1)!}G_{pp.(i-1)!}}, \tag{3}$$

where $G_{ip.(i-1)!}$ is the cross-spectrum with the correlated part of inputs up to $i-1$ removed. The residual autospectra and cross spectra are given by

$$G_{jk.r!} = G_{jk.(r-1)!} - L_{rj}G_{jr.(r-1)!}, \tag{4}$$

with L_{rj} the conditioned frequency response function

$$L_{rj} = \frac{G_{rj.(r-1)!}}{G_{rr.(r-1)!}}. \tag{5}$$

TABLE II. Conditioning sequence for a three-input system.

Step	Spectra									
1	G_{11}	G_{12}	G_{13}	G_{1p}	G_{22}	G_{23}	G_{2p}	G_{33}	G_{3p}	G_{pp}
2					$G_{22.1}$	$G_{23.1}$	$G_{2p.1}$	$G_{33.1}$	$G_{3p.1}$	$G_{pp.1}$
3						$G_{23.2!}$	$G_{2p.2!}$	$G_{33.2!}$	$G_{3p.2!}$	$G_{pp.2!}$
4									$G_{3p.3!}$	$G_{pp.3!}$

For example, in a three input, single output system, Table II shows the conditioning sequence. At step 1, the auto- and cross-spectra for the inputs and output are generated. At step 2, the spectra for $i \geq 2$ and for the output have subtracted from them the part which is correlated with the first input, generating spectra $G_{ij.1}$. At step 3, the same procedure is applied for $i \geq 3$, using Eq. (2) and (3) and the spectra from step 2. This generates spectra $G_{ij.2!}$, i.e., spectra which have had removed from them the part which is correlated with inputs 1 and 2. Finally, at step 4, the procedure is applied to the third input and to the output, generating the final spectra $G_{ij.3!}$ which have had removed the effects of all three inputs. The right hand column of Table II contains a set of output autospectra which have had successively removed the contribution from each of the inputs. To return to the concrete example, if the output signal is an at-ear noise recording and inputs 1 and 2 are measures of background noise, $G_{pp.2!}$ is the spectrum of the at-ear noise with the background noise removed, in other words, an estimate of the "true" aerodynamic noise.

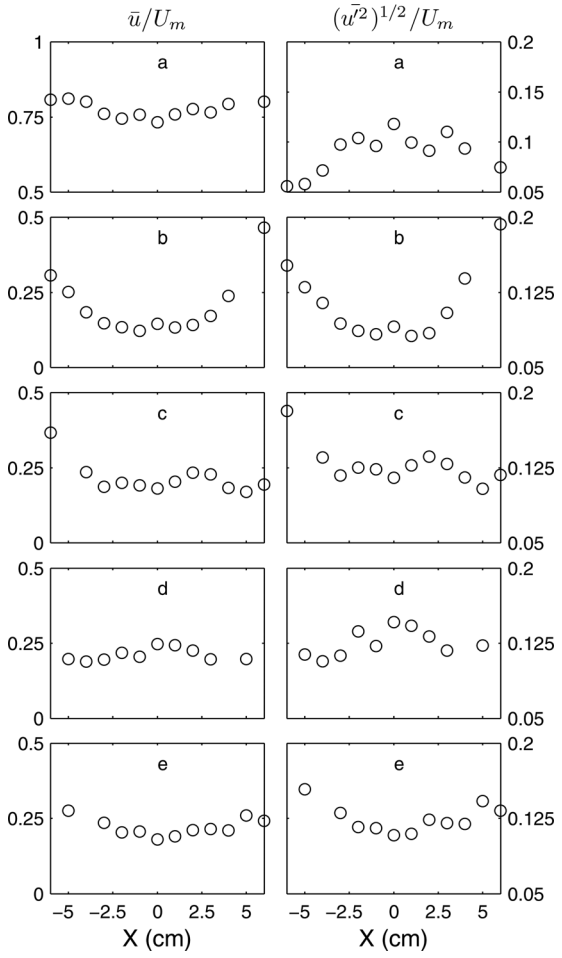

FIG. 5. Mean velocity $\bar{u}/U_m$ and turbulence intensity $(\overline{u'^2})^{1/2}/U_m$ on grid 1.

IV. WAKE FLOW FIELD

The flow statistics available from these experiments are the mean velocity magnitude and turbulence intensity. While the 55P11 hot wire probe used in this investigation is not directionally sensitive the orientation of the probe was such that the results presented here can be taken as the velocity in the free stream direction. A single hot wire probe, such as the one used in this investigation, is also poorly suited to measurements within a recirculation region. The absence of a recirculation region within the measurement planes is demonstrated by the clear transition of the mean velocity magnitudes and turbulence intensities to the values found in the downstream measurement planes. Figure 5 shows the mean velocity and turbulence intensity profiles measured at the grid locations shown in Fig. 2. These profiles show a consistently symmetric flow profile at the 5 heights measured. As a result the data from the second test grid could be mirrored to produce the full flow field behind the helmet. It should be noted that due to the curved surface of the helmet that the distance from the helmet to the measurement planes increases from the midpoint of the back surface of the helmet.

Figures 6(a) to 6(h) show the mean velocity magnitude and turbulence intensity plots for the four test locations behind the helmet. As can be seen from Figs. 6(a) and 6(b)

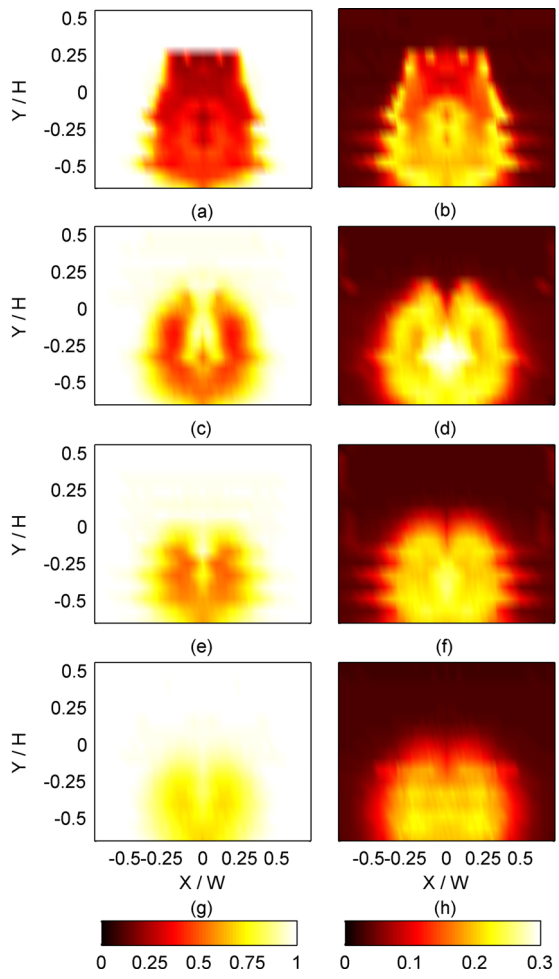

FIG. 6. (Color online) Mean velocity $\bar{u}/U_m$ and turbulence intensity $(\overline{u'^2})^{1/2}/U_m$.

the helmet shape and aerodynamic wing have succeeded in preventing separation of the free stream flow over the top surface of the helmet. High turbulence intensities are only found at or below the aerodynamic wing at the back of the helmet. A stagnation area can be found on the upper half of the helmet surface below the wing. The flow coming around the rider's neck and from the base of the helmet produces a region of high turbulence intensity close to the helmet surface.

A quarter helmet length downstream Figs. 6(c) and 6(d) show how this region of high turbulence from the lower half of the helmet increases in intensity as it mixes with the turbulence produced by the collapse of the stagnation region from the upper half of the helmet.

Figures 6(e) and 6(h) show how the entrainment of the surrounding fluid leads to lower turbulence intensities and higher mean velocities as the measurement planes move further from the helmet surface.

V. WAKE SPECTRAL RESULTS

In order to gain an understanding of possible noise sources the frequency content of the wake turbulence was investigated. Of particular interest is the nature of the turbulence produced by the various air vents and surface features of the helmet. The data were acquired at a sample rate of 44.0 kHz for 10 s and spectra were calculated at each point in the measurement grid using a window size of 8192 points providing a frequency resolution of 5.4Hz. This provides extensive spectral data for the helmet wake. Using the data from the $Z/L = 0$ measurement plane it is possible to relate the peaks seen in the spectra to the helmet features that produced them and so the data from that measurement plane is what is presented here. In order to present this information in a concise form the spectra from the 16 y-axis grid positions are presented as a single surface plot of 28 x-axis measurements. Each of these surface plots is labeled to correspond to the

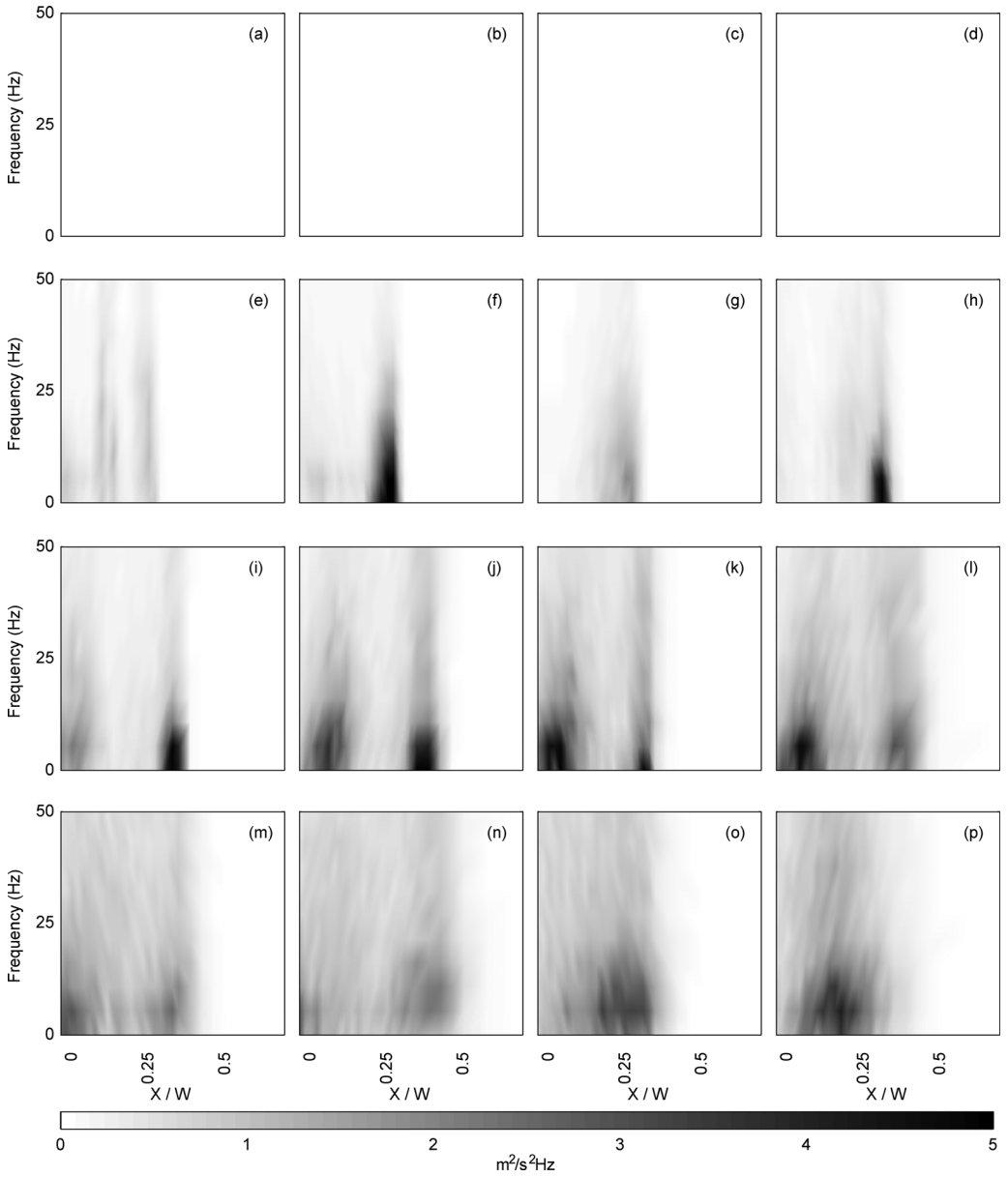

FIG. 7. Wake spectral content 0–50 Hz.

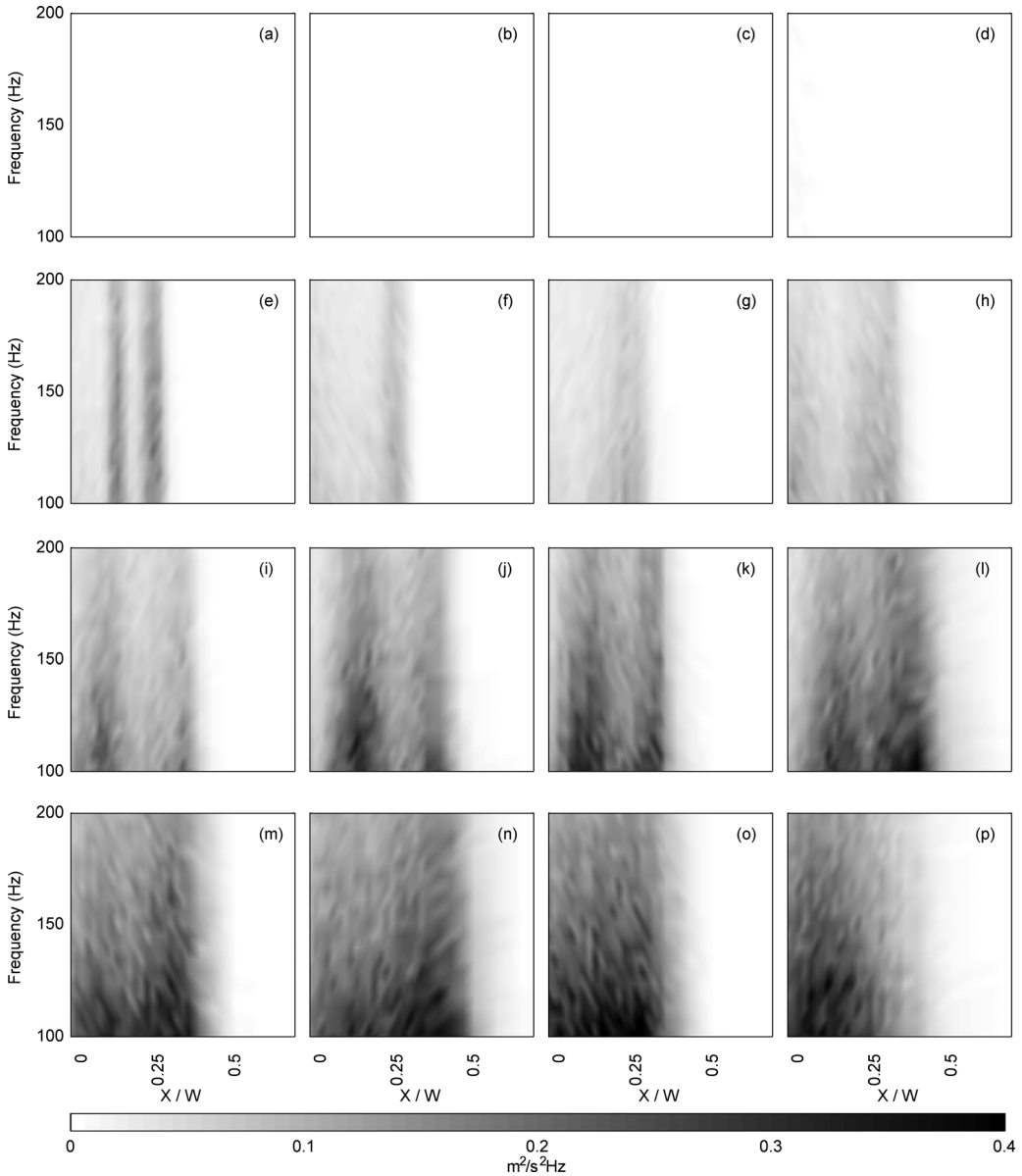

FIG. 8. Wake spectral content 100–200 Hz.

measurement planes shown in Fig. 3. This information is presented over several frequency ranges.

Figure 7 shows the 0–50 Hz range which covers the natural vortex shedding frequency of the overall helmet structure. Figure 8 shows the 100–200 Hz range where the majority of the wake energy is located and the air vents begin to produce vortices. Figure 9 shows the 500–1000 Hz range which demonstrates the wide range over which the air vents produce turbulence structures. At the flow velocity tested the helmet wake turbulence was found to be an order of magnitude lower than the free stream turbulence above 5 kHz.

As can be seen from Figs. 7(a) to 7(e) the helmet wake does not begin until below the aerodynamic wing structure. Figures 7(f) to 7(j) contain the region of strong low frequency vortex shedding from the side of the helmet. This is also the region containing the stagnation area below the aerodynamic wing as can be seen from the low amplitude spectra within this stagnation region. Figures 7(j) to 7(l) show the continuation of strong vortex shedding from the sides of the helmet combined with turbulence being generated from the center of the helmet base. Figures 7(m) to 7(p) shows the distributed wake being generated by the rider's neck and helmet base with an absence of strong vortex shedding from the helmet sides.

The 100–200 Hz range shown in Fig. 8 contains the same starting point of the wake. Figure 8(e) clearly shows the start of the turbulence being generated from the helmet air vents. It is interesting to note that flow over the top of the helmet and off the aerodynamic wing have directed the flow downward so that the air vent turbulence is detected 2 cm below the air vents at this location. The stagnation area shown in Figs. 8(f) to 8(h) contains the expected low amplitude turbulence spectra and no evidence of vortex shedding for the helmet side. As can be seen from Figs. 8(j) to 8(p) the helmet base and rider neck produce a distributed wake containing high levels of turbulence in this frequency range.

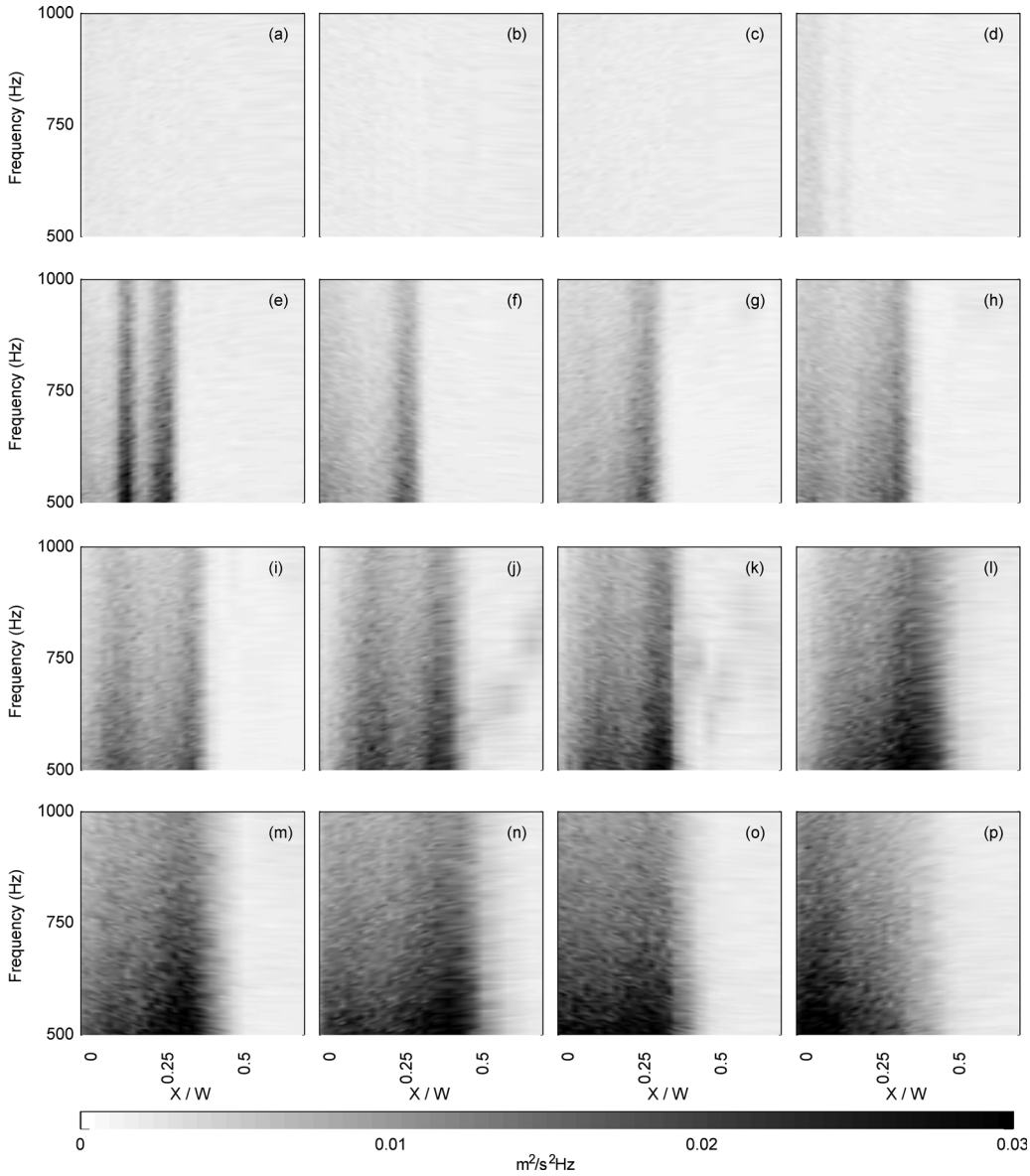

FIG. 9. Wake spectral content 500–1000 Hz.

While the amplitude of the turbulence spectra contained in the 500–1000 Hz range of Fig. 9 is 2 orders of magnitude lower than in Fig. 7 it is still clearly increased significantly from the free stream. The turbulent structures produced by the air vents are still clear in the spectra of Fig. 9(e) and these air vents have the potential to produce noise over a very wide frequency range. There is also evidence of low amplitude high frequency turbulence contained in the stagnation area although this is still significantly lower than the turbulence spectra found at the helmet base.

VI. AT-EAR NOISE

The combination of the turbulence intensity and wake spectral information can be used to indicate areas of potential interest for noise production by the helmet wake. These locations were taken to be at the air vents, the underside of the wing, vortex shedding locations for the side of the helmet and at the base of the helmet above the rider's neck. Simultaneous hot wire and at-ear microphone measurements were then acquired along a grid line covering several areas of the wake flow and at the remaining locations. These locations are marked in Fig. 10. Correlations with at-ear sound were found to be negligible for all of these test locations which implies that the wake flow is not a significant source for motorcycle noise exposure.

A second likely source of at-ear sound is the boundary layer over the helmet surface. Simultaneous hot wire and at-ear microphone measurements were taken 1 mm from the helmet surface at the key locations shown in Fig. 10. Correlations between the hot wire and at-ear microphones were again found to be negligible for these test locations. The lack of any correlation between at-ear sound and the boundary layer directly above the helmet surface is a surprising result. This may imply that the helmet lining also acts as an acoustic lining or that the contribution of the boundary layer to at-ear sound is widely distributed over the helmet surface.

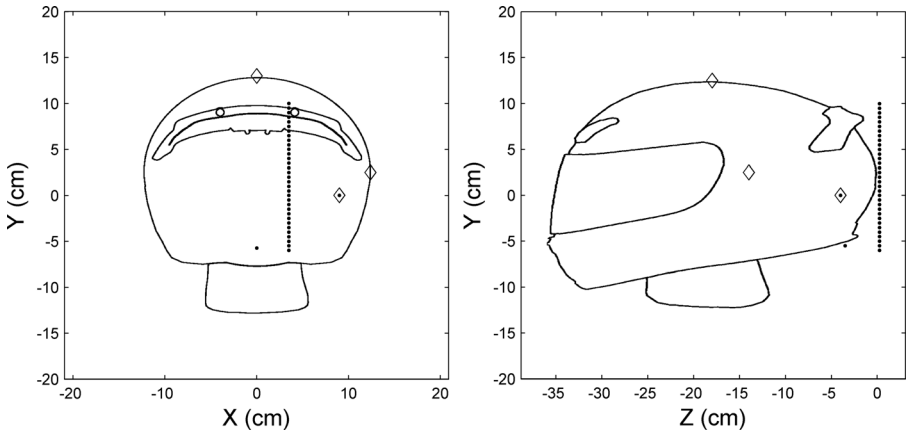

FIG. 10. Correlation measurement locations. Diamonds, boundary layer measurement; dots, wake measurement.

The final sound source investigated in these experiments is the region beneath the helmet at the chin bar. A microphone placed at the under side of the mannequin chin was used to investigate this source.

In order to check that the chin and at-ear microphones are not correlated due to being placed in the same externally imposed acoustic field, we removed the contribution of the background noise from both using the partial coherence techniques outlined in Sec. III. The signal taken from the in-tunnel microphone was used as a measurement of the external acoustic field. This was 1m from the helmet and so within a wavelength of the other two microphones for frequencies less than approximately 340 Hz. The at-ear and chin microphone signals remained correlated with this contribution removed, leading us to believe that the at-ear noise is largely connected to a source in the chin cavity region.

The chin cavity sound source was investigated as a function of wind speed and helmet angle. The wind speeds investigated corresponded to driving conditions of 40 km/h (11 m/s), 60 km/h (16.5 m/s) and 80 km/h (22 m/s) with a helmet angle of 90°, i.e. a fully upright riding condition. Figure 11 shows the partial coherence between the chin and at-ear microphones for these test conditions. As can be seen from Fig. 11 the primary effect of wind speed on the partial coherence is to move the frequency of the peak coherence from approximately 65 Hz for a speed of 40 km/h (11 m/s) to 150 Hz for a speed of 80 km/h (22 m/s). The peak amplitude of the coherence is not strongly affected.

The effect of helmet angle was investigated at a constant speed of 80 km/h (22 m/s) for the following angles: 90°, 80°, 70°, 60°, and 50°. In contrast to the effect of speed, helmet angle was a very significant factor in affecting the amplitude of the coherence producing a partial coherence greater than 0.8 in the region of 100 Hz for a helmet angle of 50°. The spectral content of the at-ear noise produced by the cavity region is affected by the helmet angle with the contribution of lower frequencies being much more significant as helmet angle decreases.

As expected, the peak frequency for the partial coherence, Fig. 11, increases with speed, with $1.7 < \mathrm{St} < 2.0$ for the peak Strouhal number over the range of speeds considered, quite different from the vortex shedding Strouhal number $\mathrm{St} = 0.18$. However when this Strouhal number is applied to the different angle configurations shown in Fig. 12 there is no collapse of the spectral peaks. No further success was achieved by any attempt to adjust the Strouhal

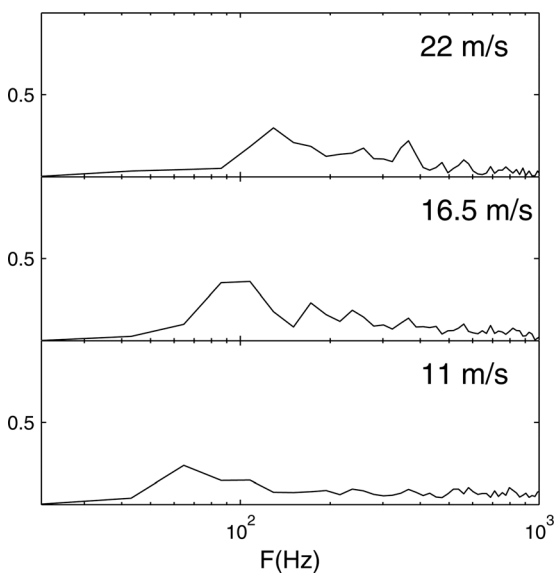

FIG. 11. Partial coherence versus speed.

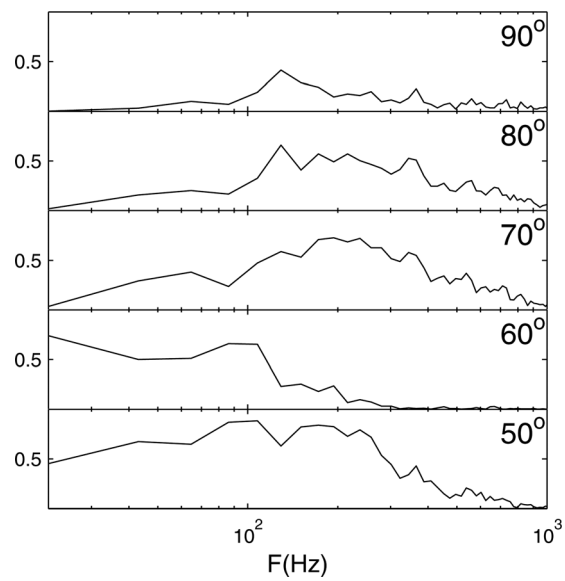

FIG. 12. Partial coherence versus head angle, $U_m = 22\mathrm{m/s}$.

number using an effective length based on the helmet angle. Using the available data there does not appear to be a single Strouhal number relationship for all helmet configurations.

These results indicate that the contribution of this flow region to the at-ear sound is both significant and dependent upon riding conditions.

VII. CONCLUSIONS

The importance of three potential motorcycle helmet noise source regions has been investigated. The helmet wake, while being shown to contain turbulence over a wide frequency range, did not prove to be a significant source of at-ear noise. An investigation of the helmet boundary layer was conducted at several locations around the helmet surface. These regions did not measurably contribute to the at-ear noise. This was surprising as one of the boundary layer regions investigated was directly above the ear location. The third potential noise source investigated was the cavity under the helmet at the chin bar. Investigations in this area were conducted using a microphone placed at the center of the mannequin chin. After conditionally removing the contribution of tunnel noise a high coherence was achieved between this region and the at-ear sound between 0 and 1000 Hz. Helmet angle and flow speed were identified as key factors governing the production of sound from this region.

The geometry of this cavity region is highly complex and will be unique to each rider and helmet combination. It is clear that it is possible to control the production of sound from this region with relatively small changes to the riding conditions. This information supports anecdotal reports of noise reduction from riders who use a neck shield to close off this cavity region.

ACKNOWLEDGMENTS

Part of this work was carried out in a project funded by the Leverhulme Trust. The authors also wish to acknowledge the assistance of Niels Bogerd of EMPA, St. Gallen, Switzerland, who supplied the helmet and to remember the contribution made by the late Paul Brühwiler who managed the COST action PROHELM, which made much of this work possible.

[1]G. A. M. Jongepier and A. van der Weerd, "Research into the noise hazard and loss of hearing in motorcycle patrols of the state police," Technical Report No. AG 89/987, RBB, Hague, Netherlands (1989), translated from Dutch.
[2]G. A. M. Jongepier and A. van der Weerd, "Practical research into application possibilities of otoplastics with motorcycle patrols of the state police," Technical Report No. AG 90/1863, RBB, Hague, Netherlands (1990), translated from Dutch.
[3]A. van der Weerd, "Comparative sound measurements with alternative motorcycles, fairings and helmets on behalf of the state police," Technical Report No. AG 90/1414, RBB, The Hague, Netherlands, Hague, Netherlands (1990), translated from Dutch.
[4]A. van der Weerd, "Comparative research into the noise hazard to motorcyclists with various fairings, shields and helmets," Technical Report No. AG 89/1705, RBB, Hague, Netherlands (1990), translated from Dutch.
[5]M. C. Lower, D. W. Hurst, A. R. Claughton, and A. Thomas, "Sources and levels of noise under motorcyclists' helmets" Proc. Inst. Acoust. **16**, 319–326 (1994).
[6]M. C. Lower, D. W. Hurst, and A. Thomas, "Noise levels and noise reduction under motorcycle helmets," in *Proceedings of Internoise* (Institute of Acoustics, St. Albans, 1996), Vol. 96, pp. 979–982.
[7]C. Jordan, O. Hetherington, A. Woodside, and H. Harvey, "Noise induced hearing loss in occupational motorcyclists," J. Environ. Health Res. **3**, 70–77 (2004).
[8]"Shock reason why we need quieter lids," Bike 18–19 (2007).
[9]S. Taneda, "Visual observations of the flow past a sphere at Reynolds numbers between 10^4 and 10^6," J. Fluid Mech. **85**, 187–192 (1978).
[10]E. Achenbach, "Experiments on the flow past spheres at very high Reynolds numbers," J. Fluid Mech. **54**, 565–575 (1972).
[11]E. Achenbach, "Vortex shedding from spheres," J. Fluid Mech. **62**, 209–221 (1974).
[12]J. Kennedy, M. Carley, N. J. Holt, and I. Walker, "The effects of windscreen flow on noise in motorcycle helmets," J. Acoust. Soc. Am. **129**, 2652 (2011).
[13]M. Carley, J. Kennedy, I. Walker, and N. J. Holt, "The experimental measurement of motorcycle noise" Proc. Meet. Acoust. **12**, 040002 (2011).
[14]M. Carley, N. Holt, and I. Walker, "Noise mechanisms in motorcycle helmet noise," Proc. Meet. Acoust. **9**, 040005 (2010).
[15]M. Carley, NASA-STD-3000: "Anthropometry and biomechanics," *Man-Systems Integration Standards: Volume I* (NASA–Johnson Space Center, Houston, TX, 1995).
[16]M. Carley and J. A. Fitzpatrick, "Spectral conditioning of propeller noise from broadband sources" J. Sound Vib. **238**, 31–49 (2000).
[17]H. W. Esmonde, J. A. Fitzpatrick, H. J. Rice, and F. Axisa, "Reduced order modelling of non-linear squeeze film dynamics," Proc. IMechE **206**, 225–238 (1992).